Research Square

Preprints are preliminary reports that have not undergone peer review.
They should not be considered conclusive, used to inform clinical practice,
or referenced by the media as validated information.

Fire disturbance drives depth-dependent soil organic carbon loss and recovery in a cold temperate forest: interactions with land-use transitions and stand structure

Jie Zhang

zhangjie111@imau.edu.cn

Inner Mongolia Agricultural University

Xiaoyu Wu

Inner Mongolia Agricultural University

Jun Guo

Inner Mongolia Agricultural University

Pei Zhou

Inner Mongolia Agricultural University

Liyuan Wang

Inner Mongolia Agricultural University

Xinyuan Du

Inner Mongolia Agricultural University

Research Article

Keywords: Fire disturbance, Burn severity, Post-fire recovery, Soil organic carbon density, Fire ecology, Carbon cycle

Posted Date: November 4th, 2026

DOI: https://doi.org/10.21203/rs.3.rs-10566139/v1

License: This work is licensed under a Creative Commons Attribution 4.0 International License.
Read Full License

Additional Declarations: No competing interests reported.

Abstract

Background

Wildfire is a primary disturbance controlling soil organic carbon density (SOCD) in cold temperate forests. However, depth-dependent fire effects are rarely evaluated together with land-use transitions and forest stand structure within a single process framework, limiting fire–carbon management in northern forests.

Methods

In Yakeshi City, western Greater Khingan Mountains, China, we integrated fire records (2000–2023), multi-temporal land use/cover data, 91 soil profiles (0–100 cm), remote-sensing stand classification, and plot surveys. Fire intensity × recovery-time effects were tested using two-way ANOVA. Carbon-loss rates were compared across fire intensities and frequencies. Land-use transition effects on 0–30 cm SOCD and stand-structure controls were quantified using ANOVA and generalized linear models (GLMs).

Results

Fire was the strongest near-surface carbon-loss process. Fire intensity, recovery time, and their interaction significantly affected stratified SOCD ($P < 0.05$). Severe fires caused the largest losses, mainly in 0–40 cm soils. One year after fire, 0–100 cm SOCD declined by approximately 27.5%; after 5 and 10 years it recovered to approximately 87.2% and 94.9% of pre-fire levels, yet severe-burn sites remained approximately 8.7% below unburned references after a decade. Single-fire 0–100 cm loss rates ranged from 13.8% to 41.3% and increased with intensity; sites burned ≥ 3 times lost approximately 35.7%. Forest-to-cropland, forest-to-grassland, and forest-to-unused-land transitions reduced 0–30 cm SOCD by 34.8%, 22.7%, and 17.4%, whereas cropland-to-forest conversion increased SOCD by 12.8%. *Larix gmelinii* had the highest 0–100 cm SOCD (4.21 kg m^{-2}), followed by *Pinus sylvestris var. mongolica* (3.83 kg m^{-2}). GLMs showed that dominant species, stand density, and canopy closure significantly regulated SOCD; a 10% increase in canopy closure was associated with + 1.09 kg m^{-2} in 0–100 cm SOCD.

Conclusions

In this cold temperate forest landscape, fire attributes shape the depth and persistence of SOCD loss and recovery, while land-use transitions and stand structure modify carbon baselines and within-forest retention. Reducing high-severity short-interval reburns, limiting forest conversion, and maintaining structurally stable coniferous stands are process-consistent priorities for soil carbon conservation, within the constraints of the chronosequence sample.

Background

Soil organic carbon (SOC) is a fundamental component of the terrestrial carbon cycle and plays a critical role in regulating ecosystem functioning and climate feedbacks (Beillouin et al. 2023; Chen et al. 2025; Song et al. 2025). Forest soils store substantial carbon stocks, and their stability is strongly influenced by vegetation characteristics, climate conditions, and disturbance regimes (Wang et al. 2023; Zhao et al. 2024). Cold temperate forests are particularly important carbon reservoirs because low temperatures and short growing seasons constrain organic-matter decomposition and promote long-term carbon accumulation. However, these ecosystems are increasingly exposed to wildfire, land-use conversion, and heterogeneous stand conditions, which may jointly alter soil carbon storage patterns.

Among disturbance agents, fire is uniquely capable of causing abrupt, vertically stratified carbon loss. Fire removes litter and fine roots, heats mineral soil, enhances post-fire erosion, and delays vegetation recovery, thereby reducing carbon inputs and accelerating losses (Certini 2005; Pellegrini et al. 2018). Fire effects are strongly depth dependent. Combustible organic matter is concentrated near the surface; consequently, light fires mainly affect the litter-dominated 0–10 cm layer, whereas severe fires can extend losses into 0–40 cm and leave multi-year legacies. Repeated burning may further truncate recovery by removing litter capital and impairing regeneration. Therefore, any process-based assessment of regional soil organic carbon density (SOCD) in fire-prone cold temperate forests must explicitly include fire attributes—intensity, frequency, and time since fire—rather than treating fire as background noise.

Land use/cover change (LUCC) is a major anthropogenic driver of SOC dynamics because it modifies vegetation cover, carbon input pathways, soil microclimate, and disturbance intensity (Huang et al. 2024; Nave et al. 2024; Li et al. 2024). Forest conversion generally causes SOC depletion, whereas restoration promotes gradual carbon recovery. Importantly, SOC responses depend on specific transition pathways; comparisons based only on static land-use categories may overlook asymmetric conversion–restoration effects. In cold temperate regions, where soil carbon accumulation is intrinsically slow, preventing forest conversion is often more effective than relying on short-term post-disturbance restoration.

Within remaining forests, stand structure represents an important internal control of SOC variation (El Mderssa et al. 2024; Luo et al. 2025; Zarafshar et al. 2024). Differences in dominant tree species, stand density, and canopy closure influence litter production, root carbon inputs, soil temperature and moisture, and microbial decomposition (Luo et al. 2025; Lang et al. 2025; Zhao et al. 2025). Nevertheless, forest land is frequently treated as a homogeneous category in regional carbon assessments, potentially ignoring considerable variation among stand types. High-carbon coniferous stands are also where many fires occur, linking stand structure to both carbon storage and fire exposure.

Although fire, LUCC, and stand structure are all recognized controls of SOC dynamics, few studies have evaluated them in a unified process-oriented framework across the soil profile in cold temperate forests of northeastern China. Existing assessments often emphasize climate or static land-cover contrasts, leaving the intensity–frequency–recovery chain of fire incompletely resolved. This gap is consequential

for fire ecology and carbon-cycle management because depth-resolved recovery trajectories determine whether burned landscapes remain carbon sources or regain sink function within policy-relevant time horizons.

From a management perspective, depth-resolved fire–carbon evidence is also needed to avoid mismatched policies: fire-control targets that ignore soil carbon recovery windows, or afforestation programs that overlook reburn risk, can both weaken net carbon outcomes. Linking fire attributes to profile SOCD therefore provides actionable thresholds for when burned landscapes are likely to regain sink function and which land/stand contexts retain more carbon capital under fire exposure.

Here we develop a fire-led assessment of SOCD in Yakeshi City, western Greater Khingan Mountains. We first quantify fire intensity, recovery time, and frequency effects on stratified SOCD; then evaluate how land-use transitions alter surface SOCD; and finally identify stand-type and stand-structure controls on within-forest SOCD. We hypothesized that (i) severe and repeated fires cause larger, deeper, and more persistent SOCD losses than light or single fires; (ii) forest conversion reduces surface SOCD more than short-term restoration recovers it; and (iii) coniferous stands with higher canopy closure and density maintain higher SOCD and thus greater carbon capital under fire risk. The intended contribution is a transferable process hierarchy for cold temperate fire–carbon management: fire attributes control loss and recovery; land-use transitions reset landscape baselines; and stand structure explains within-forest retention and exposure.

Methods

Study area

Yakeshi City is located in the western Greater Khingan Mountains, Inner Mongolia Autonomous Region, northeastern China (Figs. 1–2). The region represents a typical cold temperate forest landscape characterized by complex terrain, diverse vegetation types, and strong land-use heterogeneity. Elevation ranges from approximately 194 to 1633 m. The climate is a cold temperate continental monsoon climate, with long cold winters, short growing seasons, and uneven precipitation. Low temperatures and frequent freeze–thaw cycles strongly influence organic-matter decomposition and carbon accumulation.

Vegetation is dominated by *Larix gmelinii* forests and *Pinus sylvestris var. mongolica* forests, with birch forests, aspen forests, and mixed forests distributed in disturbed or transitional settings. Recurrent wildfire is a characteristic disturbance. Fire ignition points are often concentrated near roads, settlements, and mid-elevation forest belts (Fig. 3), providing a suitable setting for examining fire–carbon coupling under cold temperate conditions.

Data sources and preprocessing

The datasets included field soil profiles, historical SOCD spatial products, land use/cover maps, multi-source remote sensing images, field plot surveys, fire records, and auxiliary geographic data (Table 1).

All spatial datasets were processed using a consistent coordinate system and resampled to 30 m spatial resolution to ensure comparability among layers.

Field soil sampling was conducted from July to September 2023. A total of 91 sampling sites were established across the study area, covering the main land use/cover types and typical forest stand types. Soil profiles were sampled at six depth intervals: 0–10, 10–20, 20–40, 40–60, 60–80, and 80–100 cm. During sampling, site location, land use/cover type, forest stand type, dominant tree species, stand density, canopy closure, and related environmental information were recorded. Soil samples were processed in the laboratory to obtain SOC content and bulk density. Outliers were screened using the interquartile-range method and field records; skewed variables were log-transformed when necessary.

Land use/cover data for 2000, 2010, and 2023 (30 m) were obtained from the Resource and Environment Science and Data Center, Chinese Academy of Sciences, and reclassified into forest land, grassland, cropland, construction land, water bodies, and unused land (Zhang et al. 2021). Forest stand types were classified using Landsat 8 OLI and SPOT 6/7 imagery combined with field plots. Images were preprocessed through radiometric calibration, atmospheric correction, geometric correction, clipping, band combination, cloud/shadow removal, and projection unification. Spectral features, vegetation indices, texture features, and topographic variables were used with a random forest classifier (Illarionova et al. 2024; Ho et al. 2024).

Fire attributes were derived from Chinese Academy of Forestry archives for 2000–2023. After excluding agricultural burning, 331 key forest fires were retained and attributed by intensity, frequency, and recovery time. Surface fires dominated the recorded regime (78.4%), while crown fires accounted for 6.4% and were more often associated with denser pine stands. These attributes provided the chronosequence basis for evaluating depth-dependent SOCD responses.

Table 1
Summary of data sources and preprocessing methods. Datasets include remote sensing imagery, field soil profiles (n = 91), land use/cover maps (2000–2023), stand surveys, fire records, and auxiliary geographic layers. All spatial datasets were unified to a common coordinate system and resampled to 30 m where applicable.

Data type	Data source	Period	Spatial resolution / scale	Preprocessing methods
Remote sensing images	USGS; China Centre for Resources Satellite Data and Application	June-September 2023	30m,1.5m	Radiometric calibration, atmospheric correction, image registration and mosaicking, and classification
Soil organic carbon content and bulk density	Field soil sampling survey	July-September 2023	91 sampling sites	Outlier detection, standardization, normal transformation, and correction for bulk density and gravel content
Land use/cover data	Resource and Environment Science and Data Center, Chinese Academy of Sciences	2000–2023	30m	Mask extraction and reclassification
Stand structure survey data	Field plot survey and remote sensing interpretation	2023	Plot scale	Attribute organization, spatial matching, and variable extraction
Auxiliary geographic data	Administrative boundaries and DEM data	Study period	30 m or vector data	Coordinate unification, clipping, and data resampling
SOCD calculation				

SOCD was the core response variable and represents organic carbon stored per unit area within a given soil layer (Chen et al. 2023). For the ith soil layer, SOCD was calculated as $SOCD_i = SOC_i \times BD_i \times H_i \times (1 - G_i)$, where SOC_i is organic carbon content (g kg^{-1}), BD_i is bulk density (g cm^{-3}), H_i is layer thickness (cm), and G_i is the gravel volume fraction (> 2 mm). Profile SOCD (0–100 cm) was calculated as the sum of layer values. Bulk density was calibrated from ring-sampler measurements and profile fits and increased with depth from 0.85 ± 0.21 g cm^{-3} (0–10 cm) to 1.46 ± 0.16 g cm^{-3} (80–100 cm) (Table 2). Because mountainous profiles show depth heterogeneity, gravel correction was retained to reduce systematic bias.

Two depth schemes were used. For land-use comparisons and transition pathways, soils were grouped into 0–30, 30–50, and 50–100 cm layers to highlight surface, middle, and deep responses. For fire and stand analyses, the original six layers and the full 0–100 cm profile were retained. Spatial SOCD layers were generated by geostatistical interpolation after outlier screening and cross-validation, then overlaid with land-use and stand maps for extraction.

Table 2
Calibrated soil bulk density parameters of the study area by depth interval.

Depth (cm)	Bulk density (g cm^{-3})
0–10	0.85 ± 0.21
10–20	1.12 ± 0.17
20–40	1.25 ± 0.14
40–60	1.33 ± 0.11
60–80	1.41 ± 0.13
80–100	1.46 ± 0.16
Notes: Values are mean ± SD of bulk density (g cm^{-3}) measured or calibrated from ring-sampler data at 91 soil profiles. Bulk density increases with depth and was used with SOC content, layer thickness, and gravel correction to calculate layer SOCD.	
Fire disturbance analysis	

Based on burned-plot distribution for 2000–2023, agricultural burning was excluded and 11 typical burned plots were selected for a two-way ANOVA of fire intensity (light, moderate, severe) × recovery time (1, 3, 5, 10 years) on stratified SOCD (0–10 to 80–100 cm and 0–100 cm). Intensity classes were assigned from fire-record attributes describing fire behavior and post-fire vegetation damage. Recovery time was defined as the interval between the fire year and the sampling year, forming a comparable chronosequence. Intensity–frequency analysis used six fire-history plots (1986–2023) versus unburned references. Carbon-loss rate (%) was calculated as the relative SOCD reduction compared with unburned controls. Recovery status was expressed relative to pre-fire SOCD to characterize the decline–rebound–residual-deficit trajectory.

Because burned-plot sample sizes are modest, interpretation emphasizes depth patterns, severity gradients, and recovery direction rather than over-precise absolute rates or landscape-wide stock accounting. This conservative approach is appropriate for process inference under limited chronosequence replication.

Land-use transition and stand-structure analyses

Based on land use/cover maps for 2000, 2010, and 2023, we calculated area proportions, constructed transition matrices, and computed dynamic degree and transition intensity. Key pathways included forest-to-cropland, forest-to-grassland, forest-to-unused land, and cropland-to-forest transitions. These pathways were selected because they directly alter vegetation continuity, litter inputs, and soil disturbance intensity. For each selected pathway, 0–30 cm surface SOCD before and after transition was extracted, and absolute and percentage changes were calculated to evaluate asymmetric conversion–restoration effects.

Major stand types were *Larix gmelinii* forest, *Pinus sylvestris var. mongolica* forest, birch forest, aspen forest, deciduous broadleaved mixed forest, and coniferous–broadleaved mixed forest. Classification accuracy was evaluated using overall accuracy, producer's accuracy, user's accuracy, and the Kappa coefficient. One-way ANOVA was used to compare SOCD among land-use types and forest stand types, followed by multiple comparisons. Generalized linear models (GLMs) quantified effects of dominant tree species (TS), stand density (FD), canopy closure (CC), and stand age on layered and 0–100 cm SOCD. Model equations, AIC, deviance explained (D), and *P* values were reported. Ecologically meaningful and statistically supported structural variables were retained to avoid overfitting. Significance was assessed at $P < 0.05$ (highly significant at $P < 0.01$).

Results

Fire intensity, recovery time, and frequency control depth-dependent SOCD

Fire intensity, recovery time, and their interaction significantly affected stratified SOCD ($P < 0.05$; Table 3). Severe burning reduced 0–100 cm SOCD most strongly ($P < 0.01$), with losses concentrated in 0–40 cm soils. Moderate burning significantly reduced 0–40 cm SOCD ($P < 0.05$) but had limited effects below 40 cm. Light burning mainly reduced 0–10 cm SOCD ($P < 0.05$). Deep layers (40–100 cm) responded weakly to single light-to-moderate fires, consistent with limited downward heat transfer and organic-matter combustion under lower severities. The significant interaction term further indicates that recovery trajectories are not parallel across severities: severe burns systematically lag behind light burns at the same recovery time, reflecting deeper initial combustion and slower replacement of surface carbon inputs.

Table 3
Two-way ANOVA summary (F statistics) for fire intensity and recovery time effects on stratified SOCD. Factors are fire intensity (light, moderate, severe) and recovery time (1, 3, 5, 10 years) based on 11 burned chronosequence plots. Response variables are SOCD in six depth intervals and the 0–100 cm profile.

Depth (cm)	Intensity F	Recovery F	Intensity × Recovery F
0–10	12.32**	14.23**	9.17**
10–20	13.75**	15.66**	11.24**
20–40	25.14*	27.89*	23.46**
40–60	15.97	16.02	15.35
60–80	10.36	10.39	10.14
80–100	6.85	6.88	6.73
0–100	84.39**	91.07*	76.09**

Notes: Values are F statistics from two-way ANOVA. * $P < 0.05$; ** $P < 0.01$. Significant intensity × recovery interactions indicate non-parallel recovery trajectories across burn severities. Because burned-plot replication is modest, interpretation focuses on depth patterns and severity gradients rather than precise absolute rates.

Post-fire recovery was incomplete after severe fire (Table 4). Relative to pre-fire levels, 0–100 cm SOCD declined by approximately 27.5% after 1 year ($P < 0.01$). Values rebounded by year 3 but remained below pre-fire levels, indicating that three years of natural recovery were insufficient to restore pre-fire soil carbon stocks. After 5 and 10 years, 0–100 cm SOCD recovered to approximately 87.2% and 94.9% of pre-fire levels (difference between 5 and 10 years nonsignificant, $P > 0.05$), suggesting that the main recovery window is concentrated around the 5-year scale and that marginal gains diminish thereafter. Severe-burn sites were still approximately 8.7% below unburned references after 10 years ($P < 0.05$). One-year recovery ratios declined with severity (83.5%, 78.6%, and 73.1% for light, moderate, and severe burns), demonstrating a clear severity–recovery lag.

Table 4

Post-fire recovery of 0–100 cm SOCD relative to pre-fire levels. Relative SOCD status is expressed as percentage change versus pre-fire SOCD or unburned references for the indicated recovery time and severity class. Pooled one-year decline, 5- and 10-year recovery ratios, residual deficit after severe burns, and severity-specific one-year recovery ratios are summarized.

Recovery time / severity	Relative SOCD status	Statistical note
1 year (pooled)	−27.5% vs pre-fire	$P < 0.01$
3 years	Higher than 1 year, still below pre-fire	$P < 0.05$ vs 1 year
5 years	~ 87.2% of pre-fire	Main recovery window
10 years	~ 94.9% of pre-fire	ns vs 5 years
Severe burn at 10 years	~ 8.7% below unburned	$P < 0.05$
Light / moderate / severe at 1 year	83.5% / 78.6% / 73.1% of pre-fire	Severity gradient

Single-fire 0–100 cm carbon-loss rates ranged from 13.8% to 41.3% and increased with intensity ($P < 0.05$; Table 5). Severe-fire losses were concentrated in 0–40 cm; moderate fires mainly affected 0–20 cm; and light fires were largely restricted to 0–10 cm (17.6%). Repeated burning amplified profile losses: 19.4% (1 burn), 27.5% (2 burns), and 35.7% (≥ 3 burns), with 0–40 cm contributing approximately 62.3% of the ≥ 3-burn loss (Table 6). These results indicate that surface soils are most sensitive to intensity, whereas frequent reburns threaten mid-profile carbon stability and can push ecosystems toward a low-carbon, high-exposure state if reburns occur before recovery capital is rebuilt.

Table 5

Carbon-loss rates (%) under different fire intensities by soil depth. Loss rate is the relative reduction in SOCD compared with unburned controls for light, moderate, and severe fires. Values are percentages for each depth interval and for the 0–100 cm profile.

Depth (cm)	Light	Moderate	Severe	Mean
0–10	17.6c	23.1b	37.5a	26.1B
10–20	12.4b	19.2a	24.7a	18.8B
20–40	7.3b	12.6b	19.1a	13.0B
40–60	4.1a	6.5a	8.2a	6.3A
60–80	1.9a	2.8a	3.6a	2.8A
80–100	0.7a	1.1a	1.4a	1.1A
0–100	13.8c	21.7b	32.6a	22.7B

Notes: Different lowercase letters indicate significant differences among fire intensities within the same depth ($P < 0.05$). Different uppercase letters in the Mean column indicate significant differences among depth-group means ($P < 0.05$). Surface and upper-middle layers (0–40 cm) show the strongest intensity-dependent losses.

Table 6
Fire-frequency effects on 0–100 cm carbon-loss rate. Loss rates (%) are relative reductions in profile SOCD for sites with 1, 2, or ≥ 3 recorded burns compared with unburned references (six fire-history plots). The key pattern column highlights the progressive increase in profile loss and the contribution of 0–40 cm soils under repeated burning.

Fire frequency	0–100 cm loss rate (%)	Key pattern
1 burn	19.4	Baseline single-fire loss
2 burns	27.5	Significantly higher than 1 burn ($P < 0.05$)
≥ 3 burns	35.7	0–40 cm contributed ~ 62.3% of profile loss
Land-use transitions modify surface SOCD baselines		

Forest land remained dominant during 2000–2023, but forest conversion remained active (Figs. 4–6). The dynamic degree of forest land was relatively low (− 0.11%), yet forest land showed high transition intensity, with substantial annual transfers to grassland, construction land, and unused land. Construction land had the highest positive dynamic degree (+ 2.74%), followed by grassland (+ 1.51%). These patterns indicate that modest net area change can coexist with active conversion processes that are highly relevant to soil carbon dynamics.

Surface SOCD differed strongly among land-use types in the 0–30 cm layer: forest land (4.82 kg m^{-2}) > grassland (3.64) > unused land (3.05) > cropland (2.73) > water bodies (2.56) > construction land (2.14 kg m^{-2}) (Fig. 7). Differences weakened with depth, indicating that surface soil is the primary responder to land-use change.

Selected transition pathways significantly altered 0–30 cm SOCD (Table 7). Forest-to-cropland, forest-to-grassland, and forest-to-unused-land conversions reduced surface SOCD by 34.8%, 22.7%, and 17.4%, respectively, whereas cropland-to-forest conversion increased SOCD by 12.8%. Conversion losses therefore exceeded short-term restoration gains. Transitions from unused land to grassland or cropland increased surface SOCD, but absolute levels generally remained below those of stable forest land, indicating that land-class improvement does not automatically restore a high-carbon baseline. In a fire-prone landscape, such baseline shifts can amplify subsequent fire-driven carbon debts by reducing litter and root capital available for post-fire reconstruction.

Table 7

Changes in 0–30 cm SOCD before and after selected land use/cover transitions. Before/after values are mean ± SD (kg m⁻²) of surface SOCD associated with each transition pathway extracted from multi-temporal land-use overlays. Change (%) is the relative difference after transition; positive values indicate increases and negative values indicate decreases.

Transition	Before (kg m⁻²)	After (kg m⁻²)	Change (%)	Sig.
Forest → Cropland	6.37 ± 0.82	4.15 ± 0.61	−34.8	**
Forest → Grassland	6.25 ± 0.75	4.83 ± 0.58	−22.7	**
Forest → Unused land	5.92 ± 0.69	4.89 ± 0.66	−17.4	**
Cropland → Forest	3.59 ± 0.57	4.05 ± 0.62	+ 12.8	*
Cropland → Grassland	3.67 ± 0.51	4.65 ± 0.59	+ 26.7	**
Grassland → Cropland	4.42 ± 0.64	4.16 ± 0.57	−5.9	ns
Unused → Cropland	2.42 ± 0.48	2.96 ± 0.55	+ 22.3	*
Unused → Grassland	2.55 ± 0.53	3.45 ± 0.61	+ 35.1	**

Notes: Mean ± SD of 0–30 cm SOCD (kg m⁻²). * $P < 0.05$; ** $P < 0.01$; ns = not significant. Forest conversion pathways show larger absolute and relative losses than the short-term cropland-to-forest gain, indicating asymmetric conversion–restoration effects on surface carbon baselines.

Stand type and structure explain within-forest SOCD variation

Major stand types were mapped with overall accuracy 88.86% and Kappa 0.865 (Fig. 8; Table 8). *Larix gmelinii* and *Pinus sylvestris var. mongolica* forests showed relatively high producer's and user's accuracies, whereas mixed forests were more confusable because of spectral overlap. Classification uncertainty was therefore considered when interpreting SOCD contrasts among mixed stands.

Table 8
Accuracy assessment of forest stand type classification. Producer's and user's accuracies (%) are reported for six stand types mapped with a random forest classifier. Overall accuracy and Kappa summarize map performance used to support subsequent stand-level SOCD comparisons.

Forest stand type	Producer's accuracy (%)	User's accuracy (%)
Larix gmelinii forest	94.85	92.00
Pinus sylvestris var. mongolica forest	90.91	90.00
Birch forest	86.73	85.00
Aspen forest	91.67	88.00
Deciduous broadleaved mixed forest	77.78	84.00
Coniferous–broadleaved mixed forest	81.37	83.00
Overall accuracy	88.86%	—
Kappa coefficient	0.865	—

SOCD differed significantly among stand types in the 0–100 cm profile ($F = 26.274$, $P < 0.001$; Fig. 9). Mean 0–100 cm SOCD was highest in *Larix gmelinii* (4.21 kg m^{-2}), followed by *Pinus sylvestris var. mongolica* (3.83 kg m^{-2}), birch (2.74), deciduous mixed (2.62), coniferous–broadleaved mixed (2.54), and aspen (2.42 kg m^{-2}). Pairwise contrasts showed that the two coniferous types differed significantly from most broadleaved/mixed types (Table 9). Vertical profiles confirmed that coniferous advantages were strongest in surface layers and weakened with depth, consistent with litter- and fine-root-dominated controls near the surface.

Table 9

Multiple comparisons of 0–100 cm SOCD among forest stand types. Entries are pairwise differences in mean profile SOCD (kg m^{-2}) between stand types. Positive values indicate higher SOCD in the column reference type relative to the row type as arranged in the table.

Stand type	vs Larix	vs Pinus	vs Birch	vs Aspen	vs Decid. mixed
Pinus sylvestris var. mongolica	1.23*	—			
Birch	3.32**	2.09*	—		
Aspen	4.50**	3.27**	1.18*	—	
Deciduous broadleaved mixed	3.67**	2.44*	0.35	0.83	—
Coniferous–broadleaved mixed	4.22**	2.99**	0.90	0.28	0.55

Notes: Values are pairwise differences in 0–100 cm SOCD (kg m^{-2}). * $P < 0.05$; ** $P < 0.01$. Larix and Pinus stands differ significantly from most broadleaved and mixed types, consistent with higher litter persistence and cooler understory conditions in coniferous forests.

GLMs were all significant ($P < 0.001$; Fig. 10; Table 10). The 0–100 cm model explained the most deviance (D = 0.761): y = 2.670 + 0.881TS + 0.003FD + 0.109CC. Explanatory power declined with depth (D = 0.639 at 0–10 cm to 0.298 at 80–100 cm), indicating stronger structural control in surface and upper-middle soils. When other variables were held constant, each increase in dominant-species grade was associated with an average increase of 0.881 kg m^{-2} in 0–100 cm SOCD. A 10% increase in canopy closure was associated with + 1.09 kg m^{-2} in 0–100 cm SOCD; an increase of 100 trees ha^{-1} increased 0–10 and 10–20 cm SOCD by 0.2 and 0.1 kg m^{-2}, respectively. These high-carbon coniferous stands also correspond to different fire regimes (surface fires in Larix belts; higher crown-fire association in denser pine), linking structure to both carbon storage and fire exposure.

Table 10
Generalized linear model results for soil organic carbon density by soil layer. Models relate layered and 0–100 cm SOCD to dominant tree species grade (TS), stand density (FD, trees ha⁻¹), and canopy closure (CC, %). AIC is Akaike information criterion; D is deviance explained; P is model significance.

Soil layer (cm)	Model equation	AIC	D	P
0–10	y = 1.716 + 0.342TS + 0.002FD + 0.043CC	137.21	0.639	< 0.001
10–20	y = 1.225 + 0.186TS + 0.001FD + 0.028CC	123.45	0.573	< 0.001
20–40	y = 1.037 + 0.127TS + 0.017CC	105.82	0.485	< 0.001
40–60	y = 0.694 + 0.096TS + 0.012CC	96.17	0.416	< 0.001
60–80	y = 0.583 + 0.072TS	84.39	0.352	< 0.001
80–100	y = 0.415 + 0.058TS	79.61	0.298	< 0.001
0-100	y = 2.670 + 0.881TS + 0.003FD + 0.109CC	213.56	0.761	< 0.001

Notes: TS = dominant tree species grade; FD = stand density (trees ha⁻¹); CC = canopy closure (%). All models are significant at $P < 0.001$. Coefficients indicate that higher TS grade, greater canopy closure, and (in upper layers) higher stand density are associated with higher SOCD; explanatory power declines with depth.

Discussion

Fire as the core process of abrupt, depth-dependent carbon loss

Across all analyses, fire provided the clearest process signature: abrupt combustion and heating of near-surface organic pools, followed by multi-year incomplete reconstruction of carbon inputs. Mechanistically, light fires mainly consume litter and the uppermost fine-root zone, so losses are concentrated in 0–10 cm. As intensity increases, heat and combustion propagate deeper into mineral soil, removing particulate organic matter and weakening aggregation in the 10–40 cm zone; consequently, severe burns produce larger profile deficits and longer recovery lags (Certini 2005). Post-fire erosion and exposure of bare mineral surfaces can further export or redistribute surface carbon before vegetation re-establishes. In cold temperate forests, low temperatures and short growing seasons slow litter production and microbial turnover, so input replacement after severe fire is intrinsically delayed. Repeated burning intensifies this process by truncating litter capital before it accumulates, shifting a larger fraction of cumulative loss into mid-profile layers and supporting the view that fire frequency can drive decadal soil-carbon change (Pellegrini et al. 2018).

The nonsignificant difference between 5- and 10-year recovery ratios suggests that unaided recovery follows a saturating process: early rebound is driven by vegetation recolonization and renewed litter/fine-root inputs, whereas later gains diminish once the most labile surface pools are partly restored but

deeper mineral-associated losses remain. A reburn within this window can restart combustion and heating before litter and shallow-root capital are rebuilt, converting a temporary deficit into a persistent low-retention state. Thus, from a process perspective, preventing high-severity events and short-interval reburns protects the recovery pathway itself, rather than relying only on decade-scale natural reconstruction under cold temperate constraints.

Land-use transitions asymmetrically rewrite surface carbon baselines

Land-use type and transition pathways strongly modified surface SOCD by changing the continuous processes that supply and protect soil carbon. Stable forest cover maintains litterfall, root turnover, and canopy shading that keep surface soils cooler and wetter, favoring accumulation in 0–30 cm. Conversion to cropland or construction land interrupts these inputs, increases soil disturbance and aeration, and accelerates decomposition or physical removal of organic matter; unused-land and grassland transitions produce intermediate effects (Beillouin et al. 2023; Wang et al. 2023). Stronger contrasts near the surface than at depth are therefore expected, because litter, fine roots, and tillage act first on the upper profile (Li et al. 2024; Lang et al. 2025; Nave et al. 2024).

Forest-to-cropland conversion caused the largest surface SOCD decline (− 34.8%), followed by forest-to-grassland (− 22.7%) and forest-to-unused land (− 17.4%). Cropland-to-forest conversion increased SOCD by only 12.8%, consistent with an asymmetric “fast-loss, slow-rebuild” process: carbon can be rapidly oxidized or eroded after canopy removal, whereas reaccumulation depends on slower redevelopment of litter layers, root networks, and soil structure (Huang et al. 2024; Nave et al. 2024; Li et al. 2024). In fire-prone landscapes, this baseline rewrite has process consequences beyond the transition itself: lower litter and root capital reduce the materials available for post-fire reconstruction, so subsequent burns may impose larger relative carbon debts. Accordingly, preventing forest conversion protects both standing surface stocks and the recovery capacity of the soil carbon process chain.

Stand composition and structure regulate within-forest retention and fire exposure

Within forests, stand type and structure explained substantial SOCD heterogeneity through litter chemistry, rooting patterns, and microclimate control of decomposition. Needle litter from *Larix gmelinii* and *Pinus sylvestris var. mongolica* is typically more recalcitrant and decomposes more slowly than broadleaf litter, while denser canopies cool and moisten the forest floor, slowing microbial mineralization and favoring humification in cold environments (Zhao et al. 2025; Zarafshar et al. 2024; El Mderssa et al. 2024). These processes concentrate contrasts in surface and upper-middle soils, matching the depth pattern observed here. Treating forest land as a single category would therefore obscure process-level differences in carbon retention among stand types.

GLM results showed that dominant species, canopy closure, and stand density jointly regulated SOCD, with stronger effects in surface and upper-middle layers where litter and fine-root processes dominate (Luo et al. 2025; Lang et al. 2025). Higher canopy closure buffers temperature and moisture extremes and can slow decomposition; moderate increases in density can raise litter and fine-root inputs that

replenish surface SOCD. The same structural attributes, however, also shape fire behavior: denser pine stands in our records were more associated with crown-fire occurrence, implying a trade-off between carbon-retention processes and fuel continuity that promotes high-severity combustion. Process-oriented stand management therefore seeks structurally stable, high-retention coniferous stands with sufficient canopy continuity for microclimate control, while avoiding fuel arrangements that elevate crown-fire risk.

A fire–land-use–stand hierarchy for Ecological Processes

The central contribution of this study is a process hierarchy for cold temperate fire–carbon dynamics: fire attributes govern the physical–biological sequence of abrupt loss and multi-year recovery; land-use transitions rewrite the input and disturbance baselines on which that sequence operates; and stand composition and structure regulate within-forest retention while modulating fire exposure. This hierarchy clarifies why inventory-only approaches can misdiagnose carbon risk: landscapes with similar forest area may differ sharply in combustion legacy, conversion history, and stand-controlled input/decomposition regimes, producing different SOCD trajectories even under comparable climate.

Management implications follow from these processes rather than from area statistics alone: (1) prevent high-severity short-interval reburns, especially within the first decade after fire when litter and shallow-root capital remain incomplete; (2) control forest conversion because it rapidly dismantles surface carbon inputs that are slow to rebuild; and (3) maintain high-retention Larix and Pinus stands with canopy continuity that supports litter accumulation and cool understories, while limiting fuel structures linked to crown fire. Integrating fire management, land-use planning, and silviculture is therefore a process-based strategy for soil carbon conservation in this cold temperate landscape.

Limitations and future research

Several limitations should be acknowledged because they constrain the strength of process inference. First, fire chronosequence samples are modest (11 intensity–recovery plots; 6 frequency plots), so absolute loss and recovery percentages should be treated as indicative of direction and depth pattern rather than as precise regional emission factors. Second, recovery time was inferred from fire year versus sampling year rather than from repeated measurements on the same plots; unmeasured pre-fire variability and interannual climate may therefore contribute to apparent recovery trajectories. Third, fire intensity classes were assigned from archival fire-behavior and vegetation-damage attributes; we lacked direct measurements of soil heating, energy release, litter flux, erosion, or microbial responses that would more rigorously quantify causal pathways. Fourth, SOCD maps involve interpolation uncertainty in complex terrain, and mixed-forest classification accuracy was relatively lower, adding uncertainty to some stand-level contrasts. Fifth, land-use transition timing and management history (tillage intensity, grazing, harvest residues) were not fully resolved and may modulate the magnitude of LUCC-related SOCD change. Accordingly, our process hierarchy should be interpreted as a data-constrained framework for this landscape. Future work should expand burned-plot replication, couple SOCD recovery with measured fuel loads and soil temperature profiles, and apply structural equation or process-based

models to quantify direct and indirect pathways among fire, land use, and stand structure. Long-term post-fire monitoring would further validate chronosequence inferences.

Conclusions

Within the Yakeshi chronosequence and associated land-use/stand datasets, fire disturbance provides the strongest process signal of depth-dependent SOCD loss and recovery. Fire intensity, recovery time, and their interaction significantly affected stratified SOCD. Severe and repeated fires were associated with larger and more persistent losses, especially in 0–40 cm soils. One year after fire, 0–100 cm SOCD declined by approximately 27.5%; after 5 and 10 years it recovered to approximately 87.2% and 94.9% of pre-fire levels, but severe burns remained incomplete relative to unburned references after a decade. These percentages describe the sampled recovery pathway and should not be over-generalized as universal regional rates.

Land-use transitions asymmetrically modified surface carbon baselines: forest conversion substantially reduced 0–30 cm SOCD, whereas short-term cropland-to-forest restoration recovered less carbon than conversion removed. Stand composition and structure explained within-forest SOCD variation and were associated with different fire-exposure contexts, with Larix and Pinus stands showing the highest profile SOCD in our sample.

Protecting soil carbon in this cold temperate forest landscape therefore requires a process-based strategy: reduce high-severity short-interval reburns that truncate recovery, limit forest conversion that dismantles surface carbon inputs, and maintain structurally stable high-retention coniferous stands while accounting for fire-behavior trade-offs.

Abbreviations

ANOVA
analysis of variance
CAF
Chinese Academy of Forestry
CC
canopy closure
FD
stand density
GLM
generalized linear model
LUCC
land use/cover change
SOC
soil organic carbon

SOCD
soil organic carbon density
TS
dominant tree species grade.

Declarations

Funding

This work was supported by the Science and Technology Plan Project of Inner Mongolia Autonomous Region (Key Technologies of the “Space-Air-Ground-People” Multi-source Collaborative Digital Twin Platform for Forest Fire Ecological Security) [grant number 2025YFHH0067]. The funder had no role in study design, data collection and analysis, decision to publish, or preparation of the manuscript.

Data availability

The datasets supporting the conclusions of this article are available from the corresponding author on reasonable request. Fire attributes were derived from Chinese Academy of Forestry records. Land use/cover data are available from the Resource and Environment Science and Data Center, Chinese Academy of Sciences.

Declarations

Ethics approval and consent to participate

Not applicable.

Consent for publication

All authors approved the manuscript for publication in Ecological Processes.

Competing interests

The authors declare that they have no competing interests.

Author details

1 College of Energy and Transportation Engineering, Inner Mongolia Agricultural University, Hohhot 010010, China. 2 School of Transportation and Logistics Engineering, Wuhan University of Technology,

Wuhan 430070, China. 3 College of Forestry, Inner Mongolia Agricultural University, Hohhot 010010, China.

Author Contribution

JZ and PZ conceived the study. JZ and JG performed investigation and data curation. XW and XD contributed methodology and visualization. JZ, XW, and LW drafted the manuscript. All authors revised and approved the final version. JZ acquired funding and supervised the project.

Acknowledgements

We thank field and laboratory assistants and data providers who supported soil sampling and fire-record compilation.

Data Availability

The raw remote sensing datasets derived from Sentinel satellites used in this study are publicly available through the European Space Agency (ESA) Sentinel Scientific Data Hub. The processed fire risk assessment datasets generated in this research are available from the corresponding author upon reasonable request.

References

1. Beillouin D, Corbeels M, Demenois J et al (2023) A global meta-analysis of soil organic carbon in the Anthropocene. Nat Commun 14:3700. https://doi.org/10.1038/s41467-023-39338-z
2. Certini G (2005) Effects of fire on properties of forest soils: a review. Oecologia 143:1–10. https://doi.org/10.1007/s00442-004-1788-8
3. Chen J, Biswas A, Su H et al (2023) Quantifying changes in soil organic carbon density from 1982 to 2020 in Chinese grasslands using a random forest model. Front Plant Sci 14:1076902. https://doi.org/10.3389/fpls.2023.1076902
4. Chen Z, Chen L, Lu R et al (2025) A national soil organic carbon density dataset (2010–2024) in China. Sci Data 12:1480. https://doi.org/10.1038/s41597-025-05863-3
5. El Mderssa M, Elmalki M, Whalen JK et al (2024) Forest stand and soil types determine soil organic carbon storage in the Middle Atlas region of Morocco using machine learning models. All Earth 36:1–10. https://doi.org/10.1080/27669645.2024.2400432
6. Gu J, Bol R, Sun Y, Zhang H (2022) Soil carbon quantity and form are controlled predominantly by mean annual temperature along 4000 km North-South transect of Eastern China. CATENA 217:106498. https://doi.org/10.1016/j.catena.2022.106498

7. Ho VH, Morita H, Bachofer F et al (2024) Random Forest regression kriging modeling for soil organic carbon density estimation using multi-source environmental data in Central Vietnamese forests. Model Earth Syst Environ 10:7137–7158. https://doi.org/10.1007/s40808-024-02158-1
8. Huang X, Ibrahim MM, Luo Y (2024) Land use change alters soil organic carbon: constrained global patterns and predictors. Earths Future 12. https://doi.org/10.1029/2023EF004254. e2023EF004254
9. Illarionova S, Tregubova P, Shukhratov I et al (2024) Advancing forest carbon stocks' mapping using a hierarchical approach with machine learning and satellite imagery. Sci Rep 14:21032. https://doi.org/10.1038/s41598-024-71133-8
10. Lang AK, Pastore MA, Walters BF, Domke GM (2025) Bulk density calculation methods systematically alter estimates of soil organic carbon stocks in United States forests. Biogeochemistry 168:44. https://doi.org/10.1007/s10533-025-01235-6
11. Li T, Cui L, Kuhnert M et al (2024) A comprehensive review of soil organic carbon estimates: integrating remote sensing and machine learning technologies. J Soils Sediments 24:3556–3571. https://doi.org/10.1007/s11368-024-03913-8
12. Luo L, Lin K, Tao L et al (2025) Effects of stand structure and soil depth on soil properties in Cryptomeria japonica plantations. Front Glob Change 8:1548485. https://doi.org/10.3389/ffgc.2025.1548485
13. Nave LE, DeLyser K, Domke GM et al (2024) Land use change and forest management effects on soil carbon stocks in the Northeast. Carbon Balance Manag 19:5. https://doi.org/10.1186/s13021-024-00251-7
14. Pellegrini AFA, Ahlström A, Hobbie SE et al (2018) Fire frequency drives decadal changes in soil carbon and nitrogen and ecosystem productivity. Nature 553:194–198. https://doi.org/10.1038/nature24668
15. Song B, Wang M, Zhang S et al (2025) Spatial distribution, drivers, and future variation of soil organic carbon in China's ecosystems: a meta-analysis and machine-learning assessment. Ecol Indic 179:114255. https://doi.org/10.1016/j.ecolind.2025.114255
16. Wang S, Roland B, Adhikari K et al (2023) Spatial-temporal variations and driving factors of soil organic carbon in forest ecosystems of Northeast China. Ecosyst 10:100101. https://doi.org/10.1016/j.fecs.2023.100101
17. Zarafshar M, Vincent G, Korboulewsky N, Bazot S (2024) The impact of stand composition and tree density on topsoil characteristics and soil microbial activities. CATENA 234:107541. https://doi.org/10.1016/j.catena.2023.107541
18. Zhang X, Liu L, Chen X et al (2021) GLC_FCS30: global land-cover product with fine classification system at 30 m using time-series Landsat imagery. Earth Syst Sci Data 13:2753–2776. https://doi.org/10.5194/essd-13-2753-2021
19. Zhao J, Lai L, Mei Y et al (2025) Distinct roles of forest stand types in regulating soil organic carbon stability across depths. Forests 16:1585. https://doi.org/10.3390/f16101585

20. Zhao K, Yue Y, Qin F et al (2024) Carbon storage and carbon pool characteristics of *Larix gmelinii* forest in Daxing'anling, Inner Mongolia, China. Front Glob Change 7:1419023. https://doi.org/10.3389/ffgc.2024.1419023

Figures

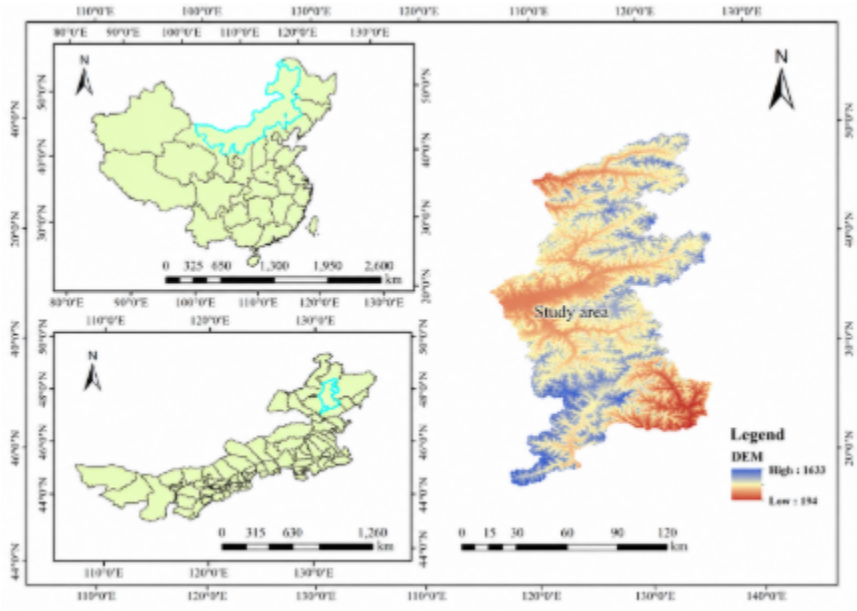


Figure 1

Location of the study area and topography of Yakeshi City. The left panel shows the position of Yakeshi City within Inner Mongolia Autonomous Region, northeastern China. The right panel shows the digital elevation model (DEM; 30 m) of the study area, where elevation ranges from approximately 194 to 1633 m. The map provides the topographic context for subsequent fire, land-use, and soil sampling overlays.

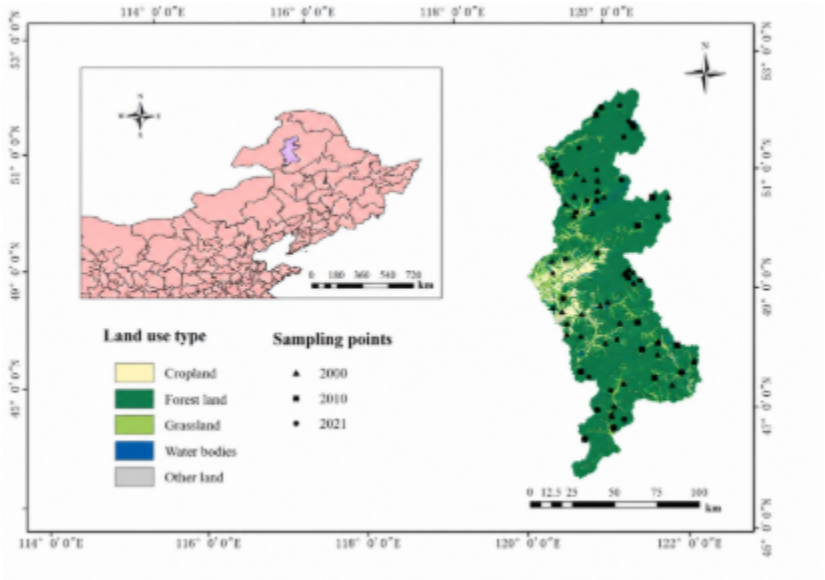


Figure 2

Land use/cover types and soil sampling sites in Yakeshi City. Land use/cover classes (forest land, grassland, cropland, construction land, water bodies, and unused land) are shown for the study landscape. Points indicate the locations of 91 soil profiles sampled to 0–100 cm. Different symbols denote sampling years as indicated in the legend. These sites provided SOC content and bulk density used to calculate stratified soil organic carbon density (SOCD).

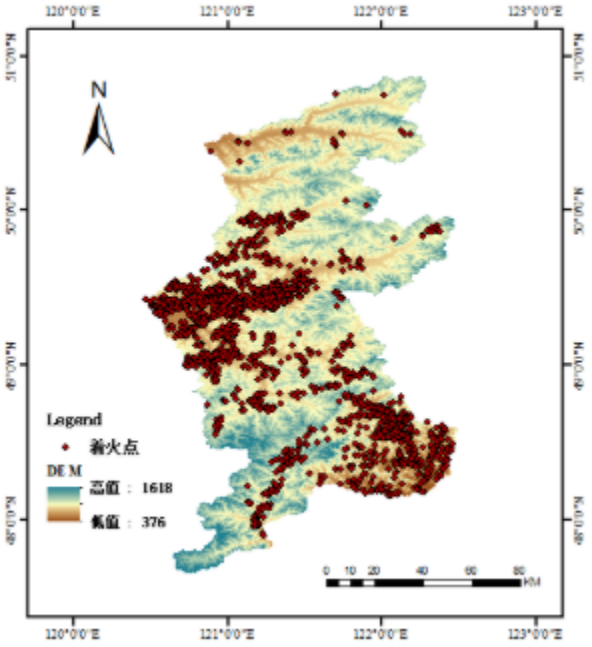


Figure 3

Spatial distribution of historical forest-fire ignition points in Yakeshi City. Ignition locations for key forest fires during 2000–2023 (agricultural burning excluded) are overlaid on the DEM. Points tend to concentrate near roads, settlements, and mid-elevation forest belts, illustrating the spatial setting of the fire chronosequence used for SOCD analyses.

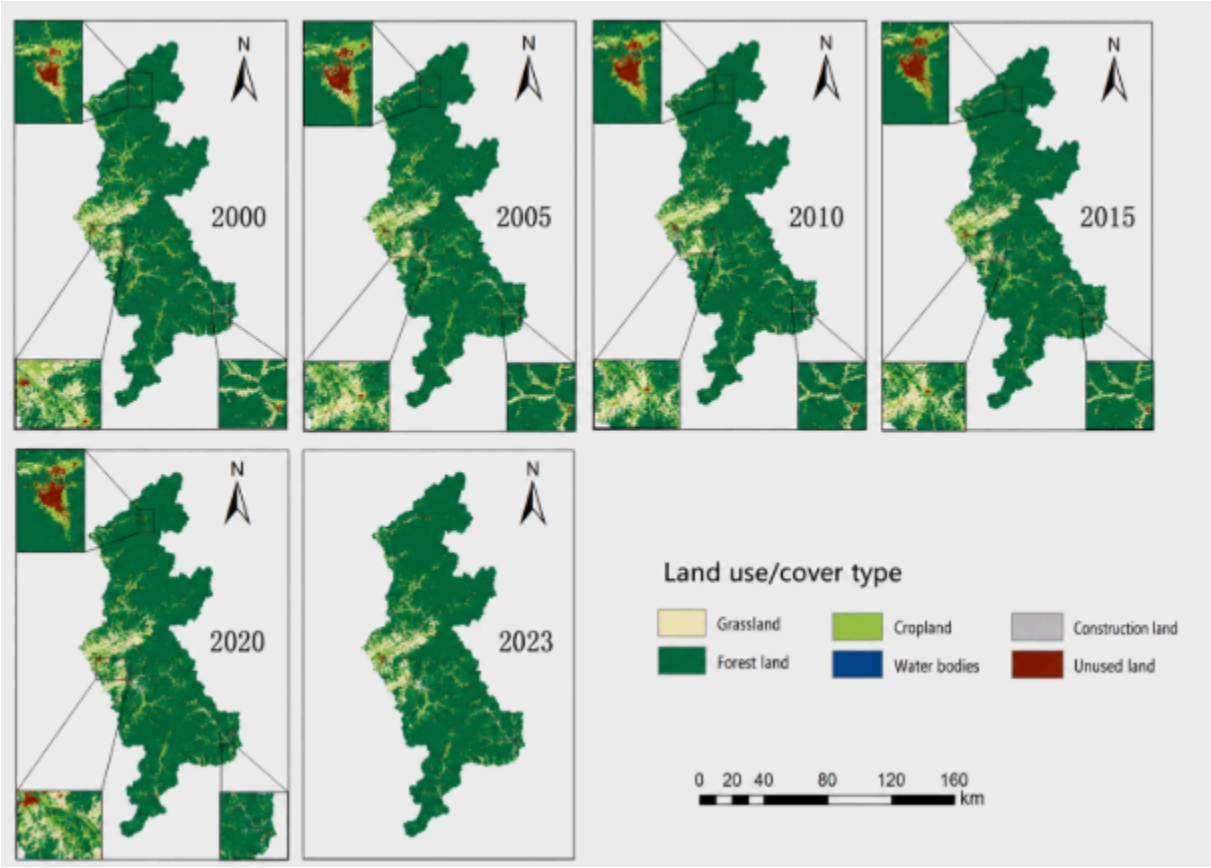


Figure 4

Spatial distribution of land use/cover in Yakeshi City in 2000, 2010, and 2023. Maps were derived from 30 m land use/cover products and reclassified into six classes. Visual comparison shows persistent forest dominance together with active local conversions among forest, grassland, cropland, construction land, and unused land over the 23-year period.

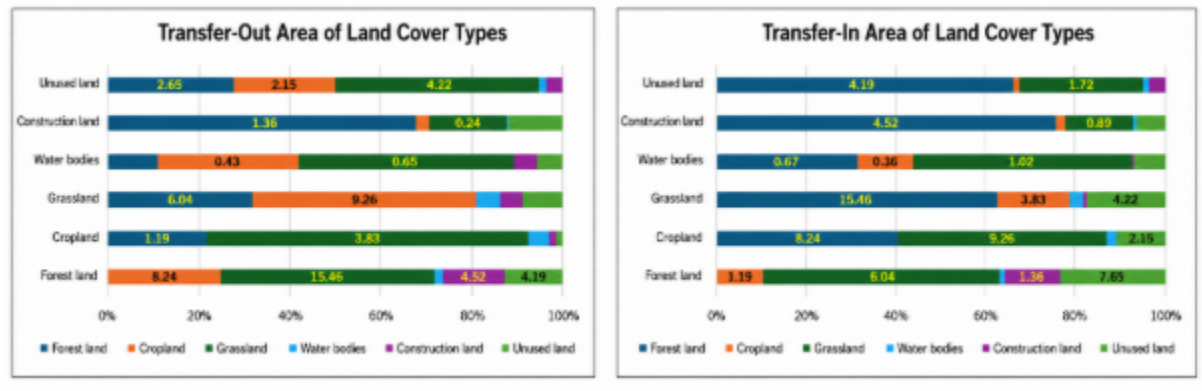


Figure 5

Transfer-out and transfer-in areas among land use/cover types in Yakeshi City, 2000–2023. Bars summarize the cumulative area transferred from each land-use class (transfer-out) and into each class (transfer-in) based on transition matrices constructed from the 2000, 2010, and 2023 maps. High

transfer intensity of forest land indicates substantial conversion activity despite relatively small net area change.

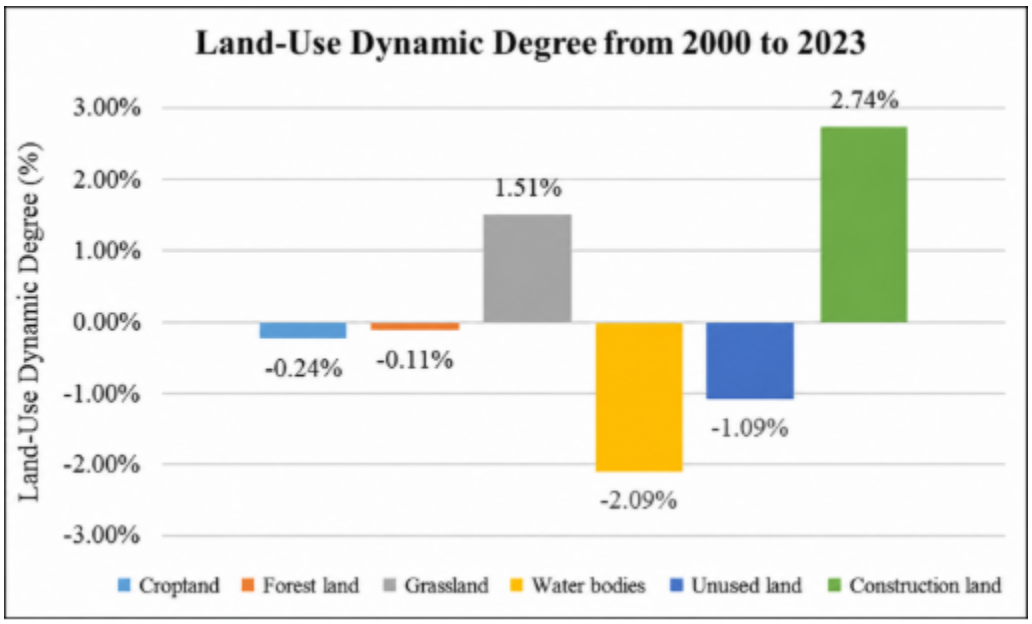


Figure 6

Land-use dynamic degree of different land use/cover types in Yakeshi City, 2000–2023. Dynamic degree quantifies the relative rate of area change for each land-use class over the study period. Positive values indicate net expansion and negative values indicate net contraction. Construction land showed the highest positive dynamic degree, whereas forest land exhibited a small negative dynamic degree accompanied by high transition intensity (see Fig. 5).

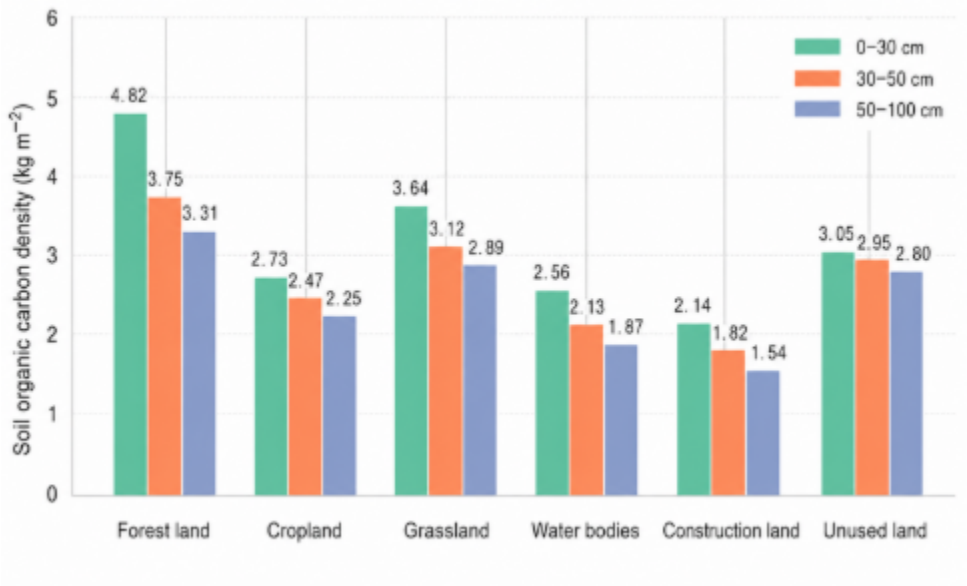


Figure 7

Stratified soil organic carbon density among land use/cover types. Bars show mean SOCD (kg m⁻²) for 0–30, 30–50, and 50–100 cm layers extracted by overlaying land-use maps with SOCD surfaces. Differences are strongest in the 0–30 cm layer (forest land > grassland > unused land > cropland > water bodies > construction land) and weaken with depth, indicating that surface soils are the primary responders to land-use change. Statistical contrasts among land-use types were evaluated by one-way ANOVA ($P < 0.05$).

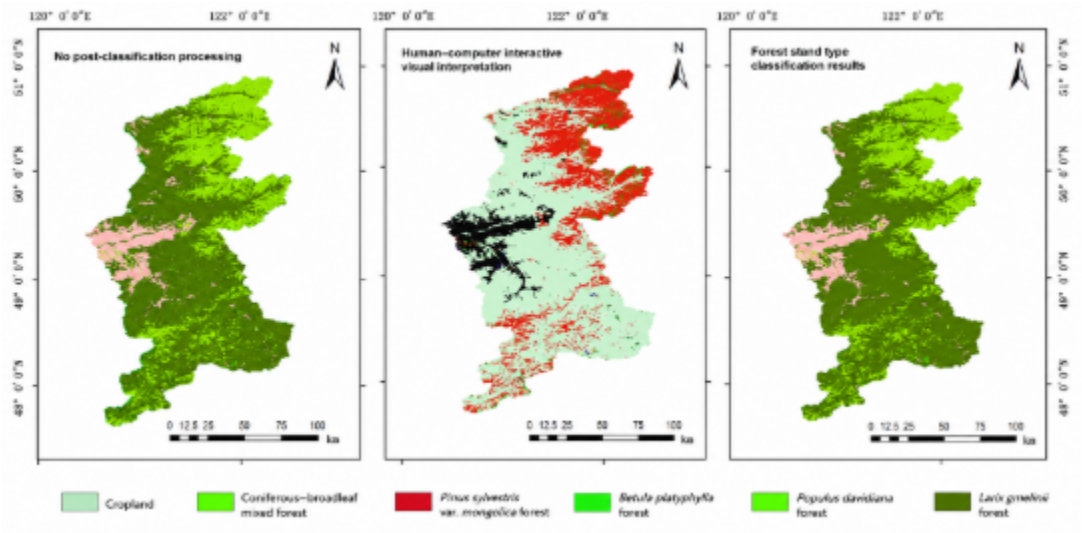


Figure 8

Spatial distribution and classification workflow of major forest stand types. Stand types (*Larix gmelinii*, *Pinus sylvestris var. mongolica*, birch, aspen, deciduous broadleaved mixed, and coniferous–broadleaved mixed forests) were mapped using Landsat 8 OLI and SPOT 6/7 imagery with a random forest classifier constrained by field plots. Overall accuracy was 88.86% and Kappa was 0.865 (Table 8). The map provided the spatial framework for extracting within-forest SOCD contrasts and stand-structure analyses.

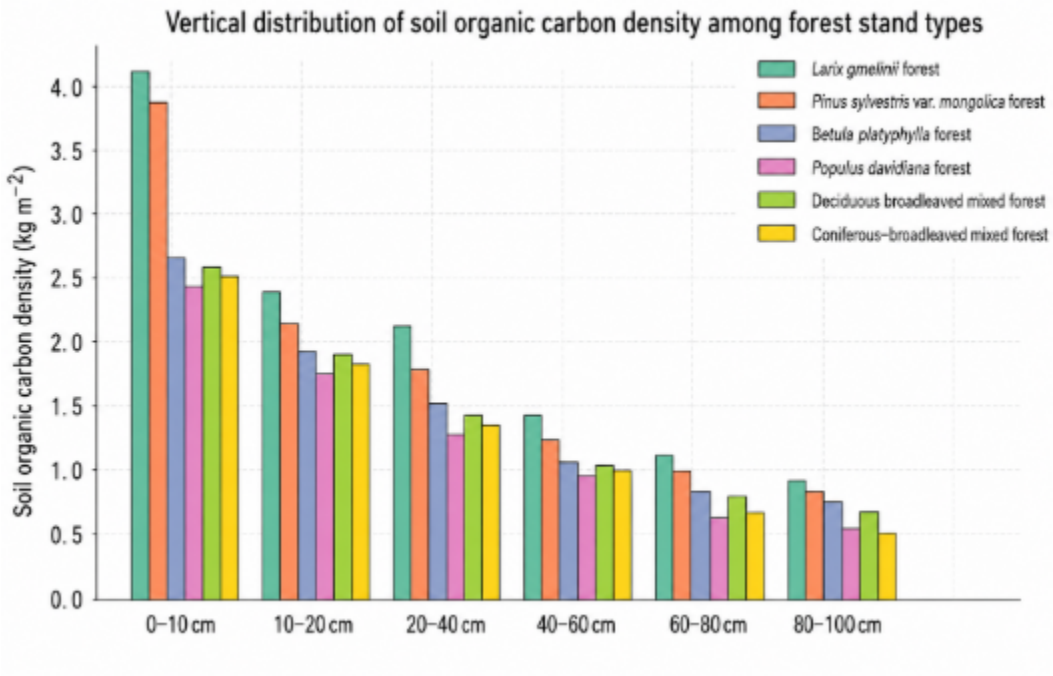


Figure 9

Vertical distribution of soil organic carbon density among forest stand types. Profiles show mean SOCD (kg m⁻²) by depth interval (0–10 to 80–100 cm) for six stand types. *Larix gmelinii* and *Pinus sylvestris var. mongolica* forests maintain higher SOCD than birch, aspen, and mixed stands, with the largest contrasts in surface and upper-middle layers. Profile-level (0–100 cm) differences were significant (one-way ANOVA, F = 26.274, $P < 0.001$); pairwise contrasts are reported in Table 9.

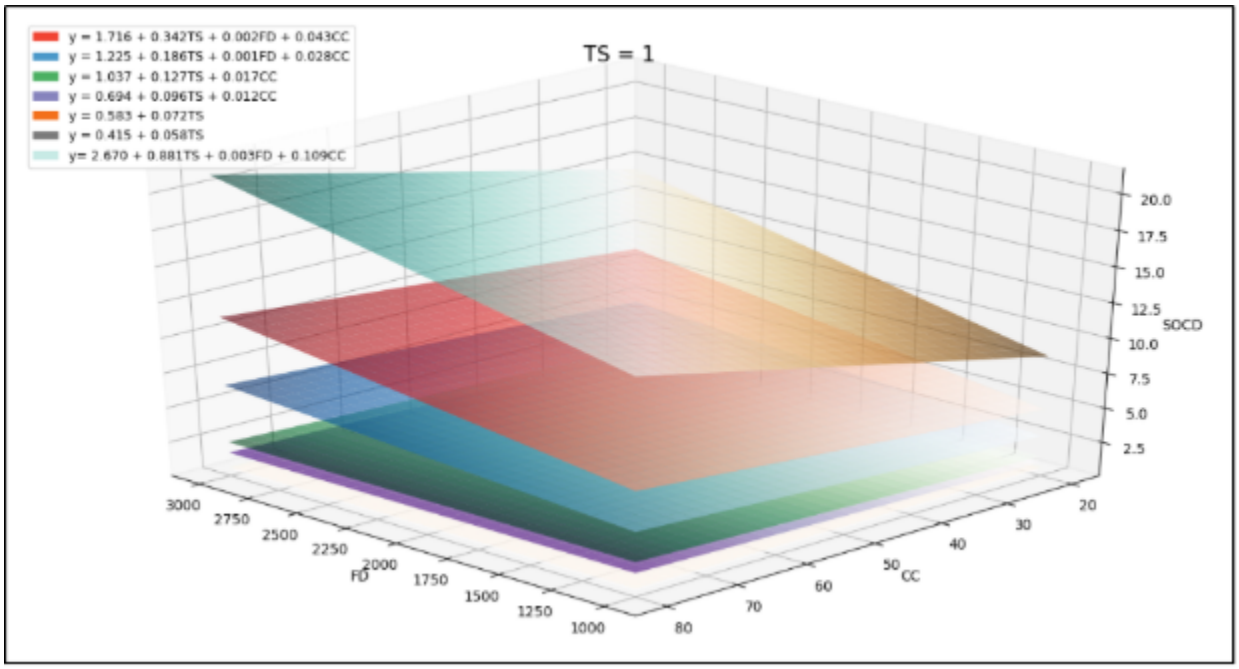


Figure 10

Effects of stand structural factors on soil organic carbon density based on generalized linear models. Panels illustrate fitted relationships between SOCD and stand structural predictors (dominant tree species grade, TS; stand density, FD, trees ha^{-1}; canopy closure, CC, %) for representative soil layers. The example surface uses TS = 1. All GLMs were significant ($P < 0.001$); model equations, AIC, deviance explained (D), and *P*values are listed in Table 10. Explanatory power was highest for the 0–100 cm profile (D = 0.761) and declined with depth.